

1    **Application of electrochemical advanced oxidation to bisphenol A**  
2            **degradation in water. Effect of sulfate and chloride ions**

3            Rutely Burgos-Castillo<sup>1\*</sup>, Ignasi Sirés<sup>2</sup>, Mika Sillanpää<sup>1</sup>, Enric Brillas<sup>2\*</sup>

4    <sup>1</sup> *Laboratory of Green Chemistry, School of Engineering Science, Lappeenranta University of*  
5    *Technology - Sammonkatu 12, FI-50130 Mikkeli, Finland*

6    <sup>2</sup> *Laboratori d'Electroquímica de Materials i del Medi Ambient, Departament de Química*  
7    *Física, Facultat de Química, Universitat de Barcelona, Martí i Franquès 1-11, 08028*  
8    *Barcelona, Spain*

9    \*Corresponding author: [rutely.burgos.castillo@lut.fi](mailto:rutely.burgos.castillo@lut.fi) (R. Burgos-Castillo)

10                            [brillas@ub.edu](mailto:brillas@ub.edu) (E. Brillas)

11 **Abstract**

12 Electrochemical oxidation with electrogenerated  $\text{H}_2\text{O}_2$  (EO-  $\text{H}_2\text{O}_2$ ), electro-Fenton (EF),  
13 photoelectro-Fenton (PEF) and solar PEF (SPEF) have been applied to mineralize bisphenol  
14 A solutions in 0.050 M  $\text{Na}_2\text{SO}_4$  or 0.008 M  $\text{NaCl}$  + 0.047 M  $\text{Na}_2\text{SO}_4$  at pH 3.0. The assays  
15 were performed in an undivided cell with a boron-doped diamond (BDD) anode and an air-  
16 diffusion cathode for continuous  $\text{H}_2\text{O}_2$  production. The PEF and SPEF processes yielded  
17 almost total mineralization due to the potent synergistic action of generated hydroxyl radicals  
18 and active chlorine, in conjunction with the photolytic action of UV radiation. The higher  
19 intensity of UV rays from sunlight explained the superior oxidation ability of SPEF. The  
20 effect of applied current density was studied in all treatments, whereas the role of bisphenol A  
21 concentration was examined in PEF. Bisphenol A abatement followed a pseudo-first-order  
22 kinetics, which was very quick in SPEF since UV light favored a large production of hydroxyl  
23 radicals from Fenton's reaction. Eight non-chlorinated and six chlorinated aromatics were  
24 identified as primary products in the chloride matrix. Ketomalonic, tartronic, maleic and  
25 oxalic acids were detected as final short-chain aliphatic carboxylic acids. The large stability of  
26 Fe(III)-oxalate complexes in EF compared to their fast photomineralization in PEF and PEF  
27 accounted for by the superior oxidation power of the latter processes.

28 *Keywords:* Bisphenol A; Electrochemical Oxidation; Electro-Fenton; Photoelectro-Fenton;  
29 Sunlight; Wastewater treatment

## 30 **1. Introduction**

31 Bisphenol A (2,2-bis(4-hydroxyphenyl)propane,  $C_{15}H_{16}O_2$ ,  $M = 228.29 \text{ g mol}^{-1}$ ) is widely  
32 used in a large variety of personal care and industrial products like face lotions/cleaners,  
33 shaving creams, shampoos, body wash/lotions, sunscreen lotions, epoxy and polycarbonate  
34 resins and plastics (Umar et al., 2013; Lane et al., 2015; Bhatnagar and Anastopoulos, 2017).  
35 This chemical is considered as an endocrine disruptor and has been related to potential  
36 metabolic diseases and reproductive effects (Rochester, 2013; Chen et al., 2017; Gassman,  
37 2017; Patel et al., 2017). These health concerns have led to the appearance of a large number  
38 of works focused on its environmental fate and stability during water treatment (Lane et al.,  
39 2015; Ebele et al., 2017; Rodriguez-Narvaez et al., 2017). Thanks to its relatively high  
40 solubility of  $300 \text{ mg}\cdot\text{L}^{-1}$  at  $25 \text{ }^\circ\text{C}$  in water (Careghini et al., 2015), bisphenol A has been  
41 detected at concentrations up to  $22 \text{ }\mu\text{g L}^{-1}$  in surface water,  $370 \text{ }\mu\text{g L}^{-1}$  in effluents from  
42 wastewater treatment plants (WWTPs) and  $1.3 \text{ }\mu\text{g L}^{-1}$  in potable tap water, as well as up to  $17$   
43  $\text{mg L}^{-1}$  in landfill leachates,  $95 \text{ mg kg}^{-1}$  in sewage sludge,  $10.5 \text{ mg kg}^{-1}$  in sediments and  $0.53$   
44  $\text{mg kg}^{-1}$  in biosolids (Corrales et al., 2015; Petrie et al., 2015; Chen et al., 2017).

45 Several authors have reported the removal of bisphenol A from water by different  
46 methods including adsorption (Bhatnagar and Anastopoulos, 2017), ozonation (Umar et al.,  
47 2013), photo-Fenton (Molkenthin et al., 2013), electrolysis with Fe(II)-activated  
48 peroxydisulfate (Yang, 2015), UV photoelectrocatalysis (Yang et al., 2016) and solar  
49 photoelectrocatalysis (Daskalaki et al., 2013; Xiang et al., 2016). The two latter techniques  
50 are electrochemical advanced oxidation processes (EAOPs) in which organic pollutants are  
51 oxidized with the in situ generated hydroxyl radical ( $\bullet\text{OH}$ ), with ability to attack most  
52 organics up to mineralization (Martínez-Huitle et al., 2015; Moreira et al., 2017). The  
53 degradation of bisphenol A has been investigated using more potent EAOPs like  
54 electrochemical oxidation (EO) and electro-Fenton (EF). Much greater oxidation ability of

55 boron-doped diamond (BDD) compared to Pt, PbO<sub>2</sub>, RuO<sub>2</sub> and glassy carbon anodes has been  
56 described (Muruganathan et al., 2008; Pereira et al., 2012). Total mineralization of 20 mg L<sup>-1</sup>  
57 bisphenol A solutions with 0.1 M Na<sub>2</sub>SO<sub>4</sub> at pH 6 was achieved by EO with BDD after 12 h  
58 of electrolysis at current density (*j*) of 35.7 mA cm<sup>-2</sup>. Phenol, hydroquinone and *p*-  
59 benzoquinone were detected as intermediates (Muruganathan et al., 2008). Similarly, Pereira  
60 et al. (2012) reported total mineralization using EO with BDD when treating solutions with  
61 150 mg L<sup>-1</sup> bisphenol A and 0.1 M Na<sub>2</sub>SO<sub>4</sub> at *j* = 30 mA cm<sup>-2</sup> for 180 min, being slightly  
62 faster upon addition of 0.026 M NaCl. Li et al. (2016) found much quicker decay of 0.020  
63 mM bisphenol A in 0.04 M NaCl as compared to 0.04 M Na<sub>2</sub>SO<sub>4</sub> by EO with a Pt/stainless  
64 steel cell at *j* between 10 and 40 mA cm<sup>-2</sup>. However, scarce mineralization and accumulation  
65 of chlorinated derivatives of the target molecule, phenol and *p*-benzoquinone were important  
66 drawbacks in the former medium. On the other hand, the EF treatment of O<sub>2</sub>-saturated  
67 solutions containing 0.70 mM bisphenol A, 3.0 mM Fe<sup>2+</sup> and 0.01 M HCl using a carbon felt  
68 cathode at cathodic potential of -0.55 V/SCE led to 82% mineralization, with formation of  
69 hydroxylated derivatives (Gözmen et al., 2003). More recently, Chmayssem et al. (2017)  
70 reported a 15% mineralization after 90 min of electrolysis of 100 mg L<sup>-1</sup> bisphenol A in 0.05  
71 M Na<sub>2</sub>SO<sub>4</sub> at pH 3.0 using an electrochemical reactor with fixed bed of glassy carbon pellets  
72 at 0.8 A. Worth mentioning, powerful Fenton-based EAOPs with photo-assisted irradiation  
73 such as photoelectro-Fenton (PEF) and solar PEF (SPEF) have not been tested yet to treat  
74 aqueous solutions of bisphenol A. Such EAOPs could be more viable processes for the  
75 remediation of real wastewater.

76 This work aims to compare the mineralization of synthetic acidic bisphenol A solutions  
77 in sulfate and chloride + sulfate containing Fe<sup>2+</sup> as catalyst by EAOPs like EF, PEF and SPEF  
78 using a BDD anode and an air-diffusion cathode for H<sub>2</sub>O<sub>2</sub> generation. Tests without any  
79 catalyst (i.e., EO process with electrogenerated H<sub>2</sub>O<sub>2</sub>) (Sirés et al., 2014) were also made to

80 clarify the role of generated hydroxyl radicals. High-performance liquid chromatography  
81 (HPLC) was used to monitor the pollutant content decay and the evolution of final carboxylic  
82 acids. Main aromatic intermediates were identified by gas chromatography-mass spectrometry  
83 (GC-MS), allowing the proposal of a reaction route for bisphenol A degradation.

## 84 **2. Experimental**

### 85 *2.1. Chemicals*

86 Bisphenol A (> 99 % purity) was purchased from Sigma-Aldrich. All the other chemicals  
87 used of HPLC or analytical grade were purchased from Fluka, Panreac, Sigma-Aldrich and  
88 Acros Organics. High quality water (Millipore Milli-Q, resistivity > 18 MΩ cm) was  
89 employed for the preparation of all solutions.

### 90 *2.2. Electrochemical experiments*

91 Solutions of 150 mL of bisphenol A in 0.050 M Na<sub>2</sub>SO<sub>4</sub> or 0.008 M NaCl + 0.047 M  
92 Na<sub>2</sub>SO<sub>4</sub> at pH 3.0, with the same conductivity of 10 mS cm<sup>-1</sup>, were treated by the different  
93 EAOPs using a cylindrical, open tank reactor under vigorous stirring. The solution was kept at  
94 35 °C by recirculation of external thermostated water through a jacket surrounding the tank  
95 reactor. The anode was a BDD thin-film electrode of 2.0 cm × 1.5 cm (exposed area of 3 cm<sup>2</sup>)  
96 purchased from NeoCoat (La-Chaux-de-Fonds, Switzerland). The cathode was a 3 cm<sup>2</sup>  
97 circular carbon-polytetrafluoroethylene (PTFE) air-diffusion electrode purchased from  
98 Sainergy Fuel Cell (Chennai, India), mounted as reported elsewhere (Guinea et al., 2010). It  
99 provided H<sub>2</sub>O<sub>2</sub> to the solution from the two-electron O<sub>2</sub> reduction via reaction (1) (Brillas et  
100 al., 2009; Sirés et al., 2014) upon injection of compressed air at 1 L min<sup>-1</sup>. The distance  
101 between both electrodes was about 1 cm.



103 The assays were conducted at constant  $j$  of 33.3-100 mA cm<sup>-2</sup> provided by an AMEL  
104 2051 potentiostat-galvanostat. EF, PEF and SPEF were run with 0.50 mM FeSO<sub>4</sub> since this  
105 concentration has been found optimal for analogous treatments of other organics (Ruiz et al.,  
106 2011). Solutions in PEF were exposed to irradiation by a Philips TL/6W/08 fluorescent (UVA  
107 light,  $\lambda_{\max} = 360$  nm) with power density of 5 W m<sup>-2</sup>, measured with a Kipp&Zonen CUV 5  
108 UV radiometer. Direct illumination in SPEF was made during the summer 2017 in our  
109 laboratory of Barcelona (latitude: 41° 23'N, longitude: 2° 10'E), with 32.6 W m<sup>-2</sup> of average  
110 UV irradiance from sunlight.

### 111 2.3. Analytical procedures

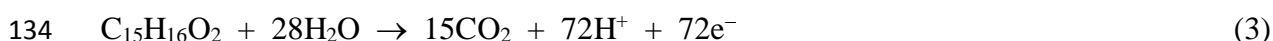
112 The solution pH was measured on a Crison GLP 22 pH-meter. All samples were filtered  
113 prior to measurements. HPLC analysis were performed by injecting 10  $\mu$ L into a Waters  
114 system composed of a 600 liquid chromatograph coupled to a 996 photodiode array detector.  
115 Bisphenol A decay was monitored by reversed-phase HPLC using a BDS Hypersil C18, 250  
116 mm  $\times$  4.6 mm, column at 25 °C and the photodiode detector set at  $\lambda = 254$  nm. The mobile  
117 phase was 30:70 (v/v) acetonitrile:water (KH<sub>2</sub>PO<sub>4</sub> 10 mM, pH 3) eluted at 1.0 mL min<sup>-1</sup>,  
118 appearing the peak of bisphenol A at retention time ( $t_r$ ) of 3.8 min. Short-linear carboxylic  
119 acids were identified by ion-exclusion HPLC using a Bio-Rad Aminex HPX 87H, 300 mm  $\times$   
120 7.8 mm, column at 35 °C, and the photodiode detector selected at  $\lambda = 210$  nm. A 4 mM H<sub>2</sub>SO<sub>4</sub>  
121 solution was eluted at 0.6 mL min<sup>-1</sup> as mobile phase. Oxalic ( $t_r = 6.8$  min), ketomalonic ( $t_r =$   
122 7.4 min), tartronic ( $t_r=7.675$ ) and maleic ( $t_r = 8.1$  min) were detected. In EF, PEF and SPEF,  
123 acetonitrile (50% in volume) was added to the samples to stop the degradation process.

124 Total organic carbon (TOC) was determined by injecting fresh samples to a Shimadzu  
125 VCSN TOC analyzer. From TOC removal ( $\Delta(\text{TOC})$ , in mg L<sup>-1</sup>) at given time ( $t$ , in h) of each  
126 test at constant applied current ( $I$ , in A), the mineralization current efficiency (MCE, in %)  
127 was calculated from Eq. (2) (Ruiz et al., 2011):

128

$$129 \quad \% \text{ MCE} = \frac{n F V \Delta(\text{TOC})}{4.32 \times 10^7 m I t} \times 100 \quad (2)$$

130 where  $F$  ( $= 96,485 \text{ C mol}^{-1}$ ) is the Faraday constant,  $V$  represents the solution volume (in L),  
131  $4.32 \times 10^7$  is a conversion factor ( $= 3,600 \text{ s h}^{-1} \times 12,000 \text{ mg C mol}^{-1}$ ) and  $m$  ( $= 15$ ) is the  
132 number of carbon atoms of bisphenol A. An  $n$ -value of 72 was accounted for the number of  
133 electrons associated with the theoretical total mineralization as follows:



135 Average data for replicated kinetic and mineralization assays are reported below, with  
136 small standard errors  $< 4\%$  within 95% confidence interval in all cases.

137 Primary aromatic intermediates formed at short electrolysis time when treating 0.556 mM  
138 bisphenol A solutions in both background electrolytes at  $j = 100 \text{ mA cm}^{-2}$  were identified by  
139 GC-MS using a NIST05 MS library. The organic components after each test were extracted  
140 with  $\text{CH}_2\text{Cl}_2$  ( $3 \times 20 \text{ mL}$ ) and the resulting solution was dried over anhydrous  $\text{Na}_2\text{SO}_4$ , filtered  
141 and concentrated up to ca. 1 mL with  $\text{N}_2$  gas (99.99% purity). The analysis was made with the  
142 equipment and conditions previously reported by us (Steter et al., 2016), using a non-polar  
143 Teknokroma Sapiens-X5 ms column.

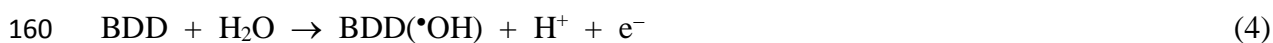
### 144 **3. Results and discussion**

#### 145 *3.1. Mineralization of bisphenol A solutions using 0.050 M $\text{Na}_2\text{SO}_4$ as the electrolyte*

146 First, solutions of 150 mL containing 0.556 mM bisphenol A ( $100 \text{ mg L}^{-1}$  TOC) in 0.050  
147 M  $\text{Na}_2\text{SO}_4$  at pH 3.0 were treated by EO- $\text{H}_2\text{O}_2$ , EF and PEF at  $j = 33.3 \text{ mA cm}^{-2}$  for 360 min.  
148 The two latter processes were run in the presence of 0.50 mM  $\text{Fe}^{2+}$ . In all cases, the initial  
149 colorless solution became brownish very rapidly, turning into yellow and being colorless  
150 again in less than 1 h. The colorful solutions at the beginning of these treatments suggest the

151 formation and fast destruction of complexes of Fe(III) with quinone-based intermediates  
152 (Feng et al., 2013; Sirés et al., 2014). Final pH values around 2.8-2.9 informed about the  
153 generation of acidic by-products such as short-linear carboxylic acids (Brillas et al., 2009; El-  
154 Gheny et al., 2013).

155 For the above trials, Fig. 1a highlights a more rapid TOC removal in the order EO-H<sub>2</sub>O<sub>2</sub>  
156 < EF < PEF, with reduction of 50.8%, 57.0% and 98.5% at 360 min. The slow but continuous  
157 TOC removal in the former EAOP can be related to the oxidation of bisphenol A and its  
158 intermediates by physisorbed BDD(•OH) originated at the BDD surface from water oxidation  
159 (Boye et al., 2002; Marselli et al., 2003; Özcan et al., 2008):



161 The larger mineralization achieved in EF can be explained by the additional production of  
162 •OH from Fenton's reaction (5) between added Fe<sup>2+</sup> and generated H<sub>2</sub>O<sub>2</sub> (Olvera-Vargas et  
163 al., 2014; Oturan and Aaron, 2014; Sirés et al., 2014), being propagated thanks to reaction (6)  
164 that involves Fe<sup>2+</sup> regeneration from cathodic Fe<sup>3+</sup> reduction.

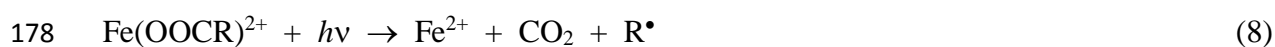


167 It can be noted that TOC removal by EF did not differ much from that in EO-H<sub>2</sub>O<sub>2</sub>  
168 (57.0% vs. 50.8%), which can be due to the formation of complexes of Fe(III), like Fe(III)-  
169 carboxylate species that are hardly removed by BDD(•OH) and •OH (Sirés et al., 2014).

170 The superiority of PEF over EF can be ascribed to the photolytic action of UVA light.  
171 This radiation promotes the formation of additional amounts of •OH along with the  
172 regeneration of Fe<sup>2+</sup> from photolysis of Fe(OH)<sup>2+</sup> via reaction (7) (Flox et al., 2007; Ruiz et  
173 al., 2011; Thiam et al., 2015b). A more crucial step for enhancing mineralization is the  
174 photodecomposition of Fe(III) complexes with intermediates, particularly some final



175 carboxylic acids according to reaction (8) (El-Ghenymy et al., 2013; Pérez et al., 2017;  
176 Moreira et al., 2017).



179 The fast photolysis of intermediates like Fe(III)-carboxylate complexes explains the  
180 almost total mineralization of bisphenol A with 98.5% TOC reduction achieved by PEF. This  
181 indicates that the combined action of BDD( $\bullet\text{OH}$ ) and  $\bullet\text{OH}$ , which are the available oxidants in  
182 EF, is strongly enhanced by the photolytic action of UVA light in PEF.

183 Moreover, the exponential decay observed in Fig. 1a for TOC abatements suggests that  
184 they agree with a pseudo-first-order kinetics and hence, the mineralization of solutions could  
185 be controlled by the generated oxidants. The apparent rate constants ( $k_{\text{TOC}}$ ) calculated from  
186 this analysis are summarized in Table 1, with their corresponding  $R^2$ . The  $k_{\text{TOC}}$ -value obtained  
187 in EO-H<sub>2</sub>O<sub>2</sub> was only 1.15-fold lower than that in EF, but much lower (6.5-fold) compared to  
188 that in PEF. This trend was verified from the MCE values calculated from Eq. (2). Fig. 1b  
189 shows that the EO-H<sub>2</sub>O<sub>2</sub> process achieved 14% of efficiency at times > 120 min, which could  
190 be related to a constant conversion of intermediates into CO<sub>2</sub>. In contrast, MCE dropped  
191 largely in EF and PEF, down to 15.2% and 26.4%, respectively, with maximal of 59.7% at  
192 120 min for the latter one. This decay in MCE at long electrolysis time can be explained by  
193 the formation of more recalcitrant molecules, along with the concomitant disappearance of  
194 organic matter (Panizza and Cerisola, 2009; Ridruejo et al., 2017).

195 The effect of an increase in  $j$  up to 100 mA cm<sup>-2</sup> on TOC removal for the treatment of  
196 0.556 mM bisphenol A by the same EAOPs along with SPEF process is depicted in Fig. 2a.  
197 From Table 1, at 240 min, the enhancement of TOC decay in the sequence EO-H<sub>2</sub>O<sub>2</sub> < EF <  
198 PEF < SPEF was found, as also verified for the profiles obtained along the electrolyses (Fig.  
199 2a). A close look to Table 1 confirms the same tendency from their  $k_{\text{TOC}}$ -values, which were

200 1.6-fold, 6.8-fold and 12.8-fold greater in EF, PEF and SPEF, respectively, as compared to  
201 EO-H<sub>2</sub>O<sub>2</sub>. Comparison of Fig. 1a and 2a, as well as TOC reductions at 240 min given in Table  
202 1, allows inferring that the increase of  $j$  from 33.3 to 100 mA cm<sup>-2</sup> accelerated the  
203 mineralization process in all cases. This upgrade can be ascribed to the concomitant increase  
204 in rate of all electrode reactions producing larger quantities of BDD(•OH) from reaction (4)  
205 and/or •OH from Fenton's reaction (5) as a result of the higher H<sub>2</sub>O<sub>2</sub> concentration produced  
206 from reaction (1). The greater generation of such hydroxyl radicals results in a quicker  
207 formation of Fe(III) complexes that can be more rapidly photolyzed by UV light in PEF and  
208 SPEF. The higher mineralization power of SPEF compared to PEF can be explained by the  
209 much greater UV power of sunlight compared to that of the commercial UVA lamp (Salazar  
210 et al., 2012; Garcia-Segura and Brillas, 2014).

211 Fig. 2b confirms the degradation ability of EAOPs from the calculated MCE values,  
212 which reached 60.4% at 40 min as maximal in SPEF, further dropping to 13.2%. Table 1 also  
213 evidences a decrease in MCE of all EAOPs when  $j$  grew from 33.3 to 100 mA cm<sup>-2</sup>, despite  
214 its greater oxidation ability. This behavior is common in these processes and can be explained  
215 by the increase in rate of parasitic reactions, thereby diminishing the relative contents of all  
216 hydroxyl radicals (Sirés et al., 2014; Thiam et al., 2015a, 2015b; Pérez et al., 2017).

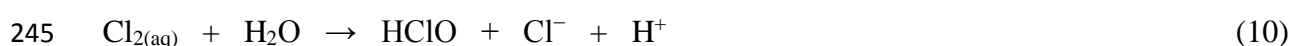
217 The influence of bisphenol A concentration on the mineralization power of EAOPs was  
218 assessed for the PEF process at 100 mA cm<sup>-2</sup>. Fig. 2c illustrates the rapid TOC removal found  
219 from 0.112 to 0.556 mM, yielding an almost total mineralization, with increasing TOC  
220 reductions from 93.2% to 96.6%, respectively. A higher bisphenol A content was thus  
221 beneficial. The same behavior can be established from the progressive rise in MCE, as can be  
222 seen in Fig. 2d and Table 1. The maximum MCE value of 31.7% was achieved at 60 min for  
223 0.556 mM and, in all cases, this parameter decreased dramatically at long time, as stated  
224 above. Nevertheless, the  $k_{\text{TOC}}$ -values slightly dropped as the initial concentration was raised

225 (Table 1), because higher amounts of TOC required larger times to be abated. Since the same  
226  $j$  was always applied, a similar production of BDD( $\bullet$ OH) and  $\bullet$ OH is expected and,  
227 consequently, the lower extent to which parasitic reactions occurred allowed that a higher  
228 MCE could be reached at high bisphenol A content (Ruiz et al., 2011; Thiam et al., 2015a,  
229 2015b; Steter et al., 2016).

### 230 3.2. Mineralization of bisphenol A solutions in chloride + sulfate medium

231 Once clarified the degradation behavior of bisphenol A in pure sulfate medium, the study  
232 was extended to a mixed electrolyte in the presence of NaCl, at pH 3.0. First assays with only  
233 0.070 M NaCl (with the same conductivity as 0.050 M Na<sub>2</sub>SO<sub>4</sub>) showed a strong inhibition of  
234 TOC removal by the EAOPs. For this reason, the effect of Cl<sup>-</sup> was studied in 0.008 M NaCl +  
235 0.047 M Na<sub>2</sub>SO<sub>4</sub>, a more realistic composition since urban and industrial wastewater usually  
236 contains both, Cl<sup>-</sup> and SO<sub>4</sub><sup>2-</sup> ions. The changes of color and pH during all electrolyses were  
237 similar to those found in 0.050 M Na<sub>2</sub>SO<sub>4</sub>.

238 Fig. 3a illustrates a rise in the oxidation ability of EAOPs in the order EO-H<sub>2</sub>O<sub>2</sub> < EF <  
239 PEF using the mixed matrix at 33.3 mA cm<sup>-2</sup>. At 240 min, for example, 23.5%, 55.2% and  
240 89.1% TOC decay was achieved for such treatments. As can be seen in Table 1, TOC  
241 abatement by EO-H<sub>2</sub>O<sub>2</sub> was slower in this medium, explained by the co-generation of active  
242 chlorine, HClO under acidic conditions, from Cl<sup>-</sup> oxidation at the BDD anode by reactions (9)  
243 and (10) (Sirés et al., 2014; Steter et al., 2016):



246 In EO-H<sub>2</sub>O<sub>2</sub>, bisphenol A and its products were then oxidized by both, BDD( $\bullet$ OH) and  
247 HClO, giving rise to recalcitrant chlorinated species (as confirmed below) that usually are  
248 more stable against radicals, eventually diminishing the oxidation power of this process. In

249 contrast, these chlorinated species were rapidly mineralized by  $\bullet\text{OH}$  in EF, as deduced from  
250 the greater mineralization ability compared to that in sulfate medium (Table 1). In PEF,  
251 smaller TOC removals were attained in the mixed electrolyte (Table 1), suggesting the  
252 photolysis of some chloro-organics. Good linear  $\ln$  TOC-time plots were obtained for these  
253 assays and the corresponding  $k_{\text{TOC}}$ -values, collected in Table 1, increased according to their  
254 relative oxidation power. The same tendency can be observed in Fig. 3b for MCE values,  
255 which decreased slightly to 10.1% and 18.9% in EO-H<sub>2</sub>O<sub>2</sub> and EF, respectively, but reached  
256 53.1% at 120 min as maximal in PEF, whereupon it dropped to 35.8% mainly due to the large  
257 loss of organic matter.

258 Fig. 4a illustrates the same trends at 100 mA cm<sup>-2</sup>, with a clear superiority of SPEF as a  
259 result of a very positive effect of UV from sunlight, which rapidly destroys the photoactive  
260 intermediates of bisphenol A. Compared with the same treatments at 33.3 mA cm<sup>-2</sup> (Fig. 3a),  
261 a notable acceleration of mineralization is evident in all cases. This enhancement with raising  
262  $j$  can also be deduced from the higher  $k_{\text{TOC}}$ -values and TOC removals at 240 min (Table 1).  
263 Again, this can be ascribed to the acceleration of all electrode reactions, producing larger  
264 amounts of BDD( $\bullet\text{OH}$ ) and/or  $\bullet\text{OH}$ , as well as of active chlorine. Despite this, the MCE  
265 values (Fig. 4b) were always much lower than those determined at 33.3 mA cm<sup>-2</sup> (Fig. 3b), as  
266 also shown in Table 1. This agrees with the concomitant increase in rate of parasitic reactions  
267 that cause the partial destruction of hydroxyl radicals. As expected, Fig. 4b shows a dramatic  
268 drop of MCE in EF, PEF and SPEF. Note that, at 100 mA cm<sup>-2</sup> in EO-H<sub>2</sub>O<sub>2</sub> and EF, higher  
269  $k_{\text{TOC}}$ -values, TOC abatements and MCE values were obtained in the mixed electrolyte as  
270 compared to pure sulfate medium (Table 1). This suggests that the large generation of  
271 BDD( $\bullet\text{OH}$ ) and/or  $\bullet\text{OH}$  in the former matrix favors their attack over chloro-derivatives  
272 leading to fast mineralization. In contrast, the data of Table 1 show a detrimental effect of Cl<sup>-</sup>  
273 in the case of PEF and SPEF, suggesting that the photoactivity of chlorinated products was

274 lower than that of non-chlorinated ones. The SPEF process yielded the fastest mineralization  
275 in both media because of the larger synergistic action of BDD( $\bullet$ OH),  $\bullet$ OH, and UV.

276 The effect of bisphenol A concentration from 0.112 to 0.556 mM on TOC removal and  
277 MCE in the mixed electrolyte at 100 mA cm<sup>-2</sup> is depicted in Fig. 4c and d, respectively.  
278 Increasing final TOC reductions from 92.0% to 96.1% with raising substrate content were  
279 found (Table 1), meaning that larger amounts of hydroxyl radicals reacted with the organic  
280 molecules rather than being destroyed by parasitic reactions. The progressively larger  
281 amounts of photoactive species thus produced can be more quickly removed upon UVA  
282 irradiation, ending in a larger mineralization. This is clear from the greater MCE values  
283 obtained at higher bisphenol A content, becoming maximal at 0.556 mM (Fig. 4d and Table  
284 1). In contrast, the corresponding  $k_{\text{TOC}}$  values shown in Table 1 underwent a slight decrease  
285 because of the slower TOC decay as the organic load in solution was greater.

### 286 3.3. Decay of bisphenol A concentration

287 It has been well established that bisphenol A obeys a pseudo-first-order decay upon the  
288 action of hydroxyl radicals using EO in 0.1 M Na<sub>2</sub>SO<sub>4</sub> (Muruganathan et al., 2008) and EF  
289 in 0.01 M HCl (Gözmen et al., 2003). To obtain more information about the reactivity of this  
290 compound in simultaneous events with BDD( $\bullet$ OH) and active chlorine, the concentration  
291 decay when treating 0.556 mM bisphenol in the mixed matrix by EO-H<sub>2</sub>O<sub>2</sub> at 100 mA cm<sup>-2</sup>  
292 was determined by HPLC. Fig. 5a shows a gradual and exponential abatement of this  
293 compound until it disappeared at 180 min. The inset panel of this figure evidences that a  
294 pseudo-first-order kinetics matched perfectly, with an apparent rate constant  $k_1 = 0.026 \text{ min}^{-1}$   
295 ( $R^2 = 0.995$ ). This is indicative of the generation in this EAOP of a small, but steady, quantity  
296 of BDD( $\bullet$ OH) and active chlorine to react with bisphenol A. On the other hand, the reaction  
297 of bisphenol A with  $\bullet$ OH in the bulk was investigated by applying the SPEF process in both  
298 media under the same experimental conditions. Fig. 5b depicts the complete bisphenol A

299 removal in only 10 min, with analogous profiles in both assays. The inset panel highlights the  
300 excellent linear straights obtained for a pseudo-first-order reaction with an average  $k_1$ -value of  
301  $0.51 \pm 0.02 \text{ min}^{-1}$  ( $R^2 \sim 0.990$ ). The much faster removal of bisphenol A in SPEF compared to  
302 EO-H<sub>2</sub>O<sub>2</sub> is in agreement with the formation of a steady concentration of •OH from Fenton's  
303 reaction (5), which is largely induced by photolytic reaction (7).

### 304 *3.4. Identification of intermediates and proposed initial reaction sequence*

305 The organic intermediates accumulated in 0.556 mM bisphenol A solutions in 0.050 M  
306 Na<sub>2</sub>SO<sub>4</sub> or 0.008 M NaCl + 0.047 M Na<sub>2</sub>SO<sub>4</sub> treated by EO-H<sub>2</sub>O<sub>2</sub> and PEF at 100 mA cm<sup>-2</sup>  
307 for times < 60 min were analyzed by GC-MS. In a given medium, similar compounds were  
308 identified regardless of the EAOP tested. Fig. 6 presents a general initial reaction sequence  
309 proposed from the 13 aromatics detected in mixed electrolyte, which could be reduced to a  
310 path with 8 non-chlorinated aromatics in 0.050 M Na<sub>2</sub>SO<sub>4</sub>. The main oxidizing species are  
311 assumed to be generated hydroxyl radicals, simplified as •OH, and active chlorine (HClO).

312 The pathway is initiated by the chlorination of bisphenol A (**1**) to yield 4,4'-  
313 isopropylidene-bis(2-chlorophenol) (**2**), along with the oxidation with cleavage of its  
314 isopropylidene group to form phenol (**3**), 4-isopropylphenol (**4**) and 4-*t*-butylphenol (**5**).  
315 Compound **3** could be further hydroxylated in C-1 and C-4 to yield catechol (**6**) and  
316 hydroquinone (**7**), respectively, or chlorinated in the same C-positions to give 2-chlorophenol  
317 (**8**) and 4-chlorophenol (**9**). Subsequent chlorination of **7** leads to chlorohydroquinone (**10**),  
318 whereas that of **8** or **9** yields 2,4-dichlorophenol (**11**). On the other hand, compound **4** was  
319 successively oxidized/hydroxylated to 4-isopropenylphenol (**12**), 4'-hydroxyacetophenone  
320 (**13**) and 2',4'-dihydroxyacetophenone (**14**). The formation of chloro-organics in the mixed  
321 electrolyte is then responsible for the slower mineralization in EO-H<sub>2</sub>O<sub>2</sub>, PEF and SPEF.

322 The pathway of Fig. 6 cannot explain the outstanding synergistic effect of UV radiation  
323 observed in PEF and SPEF, which is crucial in the mineralization processes. To clarify this,

324 the 0.556 mM bisphenol A solution in 0.050 M Na<sub>2</sub>SO<sub>4</sub> treated by EF or PEF at 100 mA cm<sup>-2</sup>  
325 was analyzed by ion-exclusion HPLC and 4 final carboxylic acids, namely oxalic,  
326 ketomalonic, tartronic and maleic, were detected. In the Fenton-based EAOPs checked, these  
327 acids form Fe(III) complexes to a large extent (Ruiz et al., 2011; El-Ghenymy et al., 2013). It  
328 was found that the three latter acids always disappeared in less than 60 min, meaning that the  
329 Fe(III) species were rapidly destroyed by BDD(<sup>•</sup>OH) and <sup>•</sup>OH. In contrast, the Fe(III)-oxalate  
330 complexes were rapidly and completely photolyzed in PEF according to reaction (8), but they  
331 were stable in EF due to their slow destruction by BDD(<sup>•</sup>OH) and <sup>•</sup>OH, with 23.5 mg L<sup>-1</sup>  
332 oxalic acid at 240 min. This represents 6.3 mg L<sup>-1</sup> TOC, accounting for 20.8% of the 30.2 mg  
333 L<sup>-1</sup> TOC of the final solution (Table 1). Therefore, UVA irradiation is so potent that not only  
334 photolyzes quickly Fe(III)-oxalate complexes, but also other photoactive intermediates to  
335 yield an almost total mineralization in PEF (Table 1).

#### 336 4. Conclusions

337 PEF and SPEF treatments with a BDD/air-diffusion cell allow an almost total  
338 mineralization of bisphenol A solutions in 0.050 M Na<sub>2</sub>SO<sub>4</sub> and 0.008 M NaCl + 0.047 M  
339 Na<sub>2</sub>SO<sub>4</sub> at pH 3.0. This is due to the synergistic action of generated oxidizing agents  
340 (BDD(<sup>•</sup>OH), <sup>•</sup>OH and/or active chlorine) along with the photolytic action of UV radiation.  
341 The most powerful EAOP was SPEF, as result of the higher UV power provided by sunlight.  
342 The increase of *j* accelerated the mineralization, but with lower MCE, whereas the rise of  
343 bisphenol A concentration yielded greater mineralization and MCE in PEF. The bisphenol A  
344 decay always obeyed a pseudo-first-order kinetics. GC-MS analysis of treated solutions  
345 revealed the generation of 8 non-chlorinated and 6 chlorinated primary aromatics in the mixed  
346 electrolyte, demonstrating the simultaneous attack of hydroxyl radicals and chlorine active

347 over bisphenol A and its products. Ketomalonic, tartronic, maleic and oxalic acids were  
348 detected as final short-chain aliphatic intermediates.

### 349 **Acknowledgements**

350 The authors thank financial support from project CTQ2016-78616-R (AEI/FEDER, EU)  
351 and the fellowship awarded to R. Burgos-Castillo granted from a project supported by the  
352 Finnish Funding Agency for Innovation.

### 353 **References**

- 354 Bhatnagar, A., Anastopoulos, I., 2017. Adsorptive removal of bisphenol A (BPA) from  
355 aqueous solution: A review. *Chemosphere* 168, 885-902.
- 356 Boye, B., Michaud, P.A., Marselli, B., Dieng, M.M., Brillas, E., Comninellis, C., 2002.  
357 Anodic oxidation of 4-chlorophenoxyacetic acid on synthetic boron-doped diamond  
358 electrode. *New Diamond Frontier Carbon Technol.* 12, 63-72.
- 359 Brillas, E., Sirés, I., Oturan, M.A., 2009. Electro-Fenton and related electrochemical  
360 technologies based on Fenton's reaction chemistry. *Chem. Rev.* 109, 6570-6631.
- 361 Careghini, A., Mastorgio, A.F., Saponaro, S., Sezenna, E., 2015. Bisphenol A, nonylphenols,  
362 benzophenones, and benzotriazoles in soils, groundwater, surface water, sediments, and  
363 food: A review. *Environ. Sci. Pollut. Res.* 22, 5711-5741.
- 364 Chen, J., Saili, K.S., Liu, Y., Li, L., Zhao, Y., Jia, Y., Bai, C., Tanguay, R.L., Dong, Q.,  
365 Huang, C., 2017. Developmental bisphenol A exposure impairs sperm function and  
366 reproduction in zebrafish. *Chemosphere* 169, 262-270.
- 367 Chmayssem, A., Taha, S., Hauchard, D., 2017. Scaled-up electrochemical reactor with a fixed  
368 bed three-dimensional cathode for electro-Fenton process: Application to the treatment  
369 of bisphenol A. *Electrochim. Acta* 225, 435-442.



370 Corrales, J., Kristofco, L.A., Steele, W.B., Yates, B.S., Breed, C.S., Williams, E.S., Brooks,  
371 B.W., 2015. Global assessment of bisphenol a in the environment: Review and analysis  
372 of its occurrence and bioaccumulation. *Dose Response* 13, 1559325815598308.

373 Daskalaki, V.M., Fulgione, I., Frontistis, Z., Rizzo, L., Mantzavinos, D., 2013. Solar light-  
374 induced photoelectrocatalytic degradation of bisphenol-A on TiO<sub>2</sub>/ITO film anode and  
375 BDD cathode. *Catal. Today* 209, 74-78.

376 Ebele, A.J., Abou-Elwafa, M.A., Harrad, S., 2017. Pharmaceuticals and personal care  
377 products (PPCPs) in the freshwater aquatic environment. *Emerg. Contam.* 3, 1-16.

378 El-Ghenemy, A., Oturan, N., Oturan, M.A., Garrido, J.A., Cabot, P.L., Centellas, F.,  
379 Rodríguez, R.M., Brillas, E., 2013. Comparative electro-Fenton and UVA photoelectro-  
380 Fenton degradation of the antibiotic sulfanilamide using a stirred BDD/air-diffusion  
381 tank reactor. *Chem. Eng. J.* 234, 115-123.

382 Feng, L., Van Hullebusch, E.D., Rodrigo, M.A., Esposito, G., Oturan, M.A., 2013. Removal  
383 of residual anti-inflammatory and analgesic pharmaceuticals from aqueous systems by  
384 electrochemical advanced oxidation processes. A review. *Chem. Eng. J.* 228, 944-964.

385 Flox, C., Garrido, J.A., Rodríguez, R.M., Cabot, P.L., Centellas, F., Arias, C., Brillas, E.,  
386 2007. Mineralization of herbicide mecoprop by photoelectro-Fenton with UVA and  
387 solar light. *Catal. Today* 129, 29-36.

388 Garcia-Segura, S., Brillas, E., 2014. Advances in solar photoelectro-Fenton: Decolorization  
389 and mineralization of the Direct Yellow 4 diazo dye using an autonomous solar pre-  
390 pilot plant. *Electrochim. Acta* 140, 384-395.

391 Gassman, N.R., 2017. Induction of oxidative stress by bisphenol A and its pleiotropic effects.  
392 *Environ. Mol. Mutagen.* 58, 60-71.

393 Gözmen, B., Oturan, M.A., Oturan, N., Erbatur, O., 2003. Indirect electrochemical treatment  
394 of bisphenol A in water via electrochemically generated Fenton's reagent. *Environ. Sci.*  
395 *Technol.* 37, 3716-3723.

396 Guinea, E., Garrido, J.A., Rodríguez, R.M., Cabot, P.L., Arias, C., Centellas, F., Brillas, E.,  
397 2010. Degradation of the fluoroquinolone enrofloxacin by electrochemical advanced  
398 oxidation processes based on hydrogen peroxide electrogeneration. *Electrochim. Acta* 55,  
399 2101-2115.

400 Lane, R.F., Adams, C.D., Randtke, S.J., Carter, R.E., 2015. Bisphenol diglycidyl ethers and  
401 bisphenol A and their hydrolysis in drinking water. *Water Res.* 72, 331-339.

402 Li, H., Long, Y., Wang, Y., Zhu, C., Ni, J., 2016. Electrochemical degradation of bisphenol A  
403 in chloride electrolyte—Factor analysis and mechanisms study. *Electrochim. Acta* 222,  
404 1144-1152.

405 Marselli, B., Garcia-Gomez, J., Michaud, P.A., Rodrigo, M.A., Comninellis, C., 2003.  
406 Electrogeneration of hydroxyl radicals on boron-doped diamond electrodes. *J.*  
407 *Electrochem. Soc.* 150, D79-D83.

408 Martínez-Huitle, C.A., Rodrigo, M.A., Sirés, I., Scialdone, O., 2015. Single and coupled  
409 electrochemical processes and reactors for the abatement of organic water pollutants: A  
410 critical review. *Chem. Rev.* 115, 13362–13407.

411 Molkenhain, M., Olmez-Hanci, T., Jekel, M.R., Arslan-Alaton, I., 2013. Photo-Fenton-like  
412 treatment of BPA: Effect of UV light source and water matrix on toxicity and  
413 transformation products. *Water Res.* 47, 5052-5064.

414 Moreira, F.C., Boaventura, R.A.R., Brillas, E., Vilar, V.J.P., 2017. Electrochemical advanced  
415 oxidation processes: A review on their application to synthetic and real wastewaters.  
416 *Appl. Catal. B: Environ.* 202, 217-261.

417 Muruganathan, M., Yoshihara, S., Rakuma, T., Shirakashi, T., 2008. Mineralization of  
418 bisphenol A (BPA) by anodic oxidation with boron-doped diamond (BDD) electrode. *J.*  
419 *Hazard. Mater.* 154, 213-220.

420 Olvera-Vargas, H., Oturan, N., Brillas, E., Buisson, D., Esposito, G., Oturan, M.A., 2014.  
421 Electrochemical advanced oxidation for cold incineration of the pharmaceutical  
422 ranitidine: Mineralization pathway and toxicity evolution. *Chemosphere* 117, 644-651.

423 Oturan, M.A., Aaron, J.J., 2014. Advanced oxidation processes in water/wastewater  
424 treatment: Principles and applications. A review. *Crit. Rev. Environ. Sci. Technol.* 44,  
425 2577-2641.

426 Özcan, A., Şahin, Y., Koparal, A.S., Oturan, M.A., 2008. Protham mineralization in aqueous  
427 medium by anodic oxidation using boron-doped diamond anode. Experimental  
428 parameters' influence on degradation kinetics and mineralization efficiency. *Water Res.*  
429 42, 2889-2898.

430 Panizza, M., Cerisola, G., 2009. Direct and mediated anodic oxidation of organic pollutants.  
431 *Chem. Rev.* 109, 6541-6569.

432 Patel, S., Brehm, E., Gao, L., Rattan, S., Ziv-Gal, A., Flaws, J.A., 2017. Bisphenol A  
433 exposure, ovarian follicle numbers, and female sex steroid hormone levels: results from  
434 a CLARITY-BPA study. *Endocrinology* 158, 1727-1738.

435 Pereira, G.F., Rocha-Filho, R.C., Bocchi, N., Biaggio, S.R., 2012. Electrochemical  
436 degradation of bisphenol A using a flow reactor with a boron-doped diamond anode.  
437 *Chem. Eng. J.* 198-199, 282-288.

438 Pérez, T., Sirés, I., Brillas, E., Nava, J.L., 2017. Solar photoelectro-Fenton flow plant  
439 modeling for the degradation of the antibiotic erythromycin in sulfate medium.  
440 *Electrochim. Acta* 228, 45-56.

441 Petrie, B., Barden, R., Kasprzyk-Hordern, B., 2015. A review on emerging contaminants in  
442 wastewaters and the environment: Current knowledge, understudied areas and  
443 recommendations for future monitoring. *Water Res.* 72, 3-27.

444 Ridruejo, C., Salazar, C., Cabot, P.L., Centellas, F., Brillas, E., Sirés, I., 2017.  
445 Electrochemical oxidation of anesthetic tetracaine in aqueous medium. Influence of the  
446 anode and matrix composition. *Chem. Eng. J.* 326, 811-819.

447 Rochester, J.R., 2013. Bisphenol A and human health: A review of the literature. *Reprod.*  
448 *Toxicol.* 42, 132-155.

449 Rodriguez-Narvaez, O.M., Peralta-Hernandez, J.M., Goonetilleke, A., Bandala, E.R., 2017.  
450 Treatment technologies for emerging contaminants in water: A review. *Chem. Eng. J.*  
451 323, 361-380.

452 Ruiz, E.J., Hernández-Ramírez, A., Peralta-Hernández, J.M., Arias, C., Brillas, E., 2011.  
453 Application of solar photoelectro-Fenton technology to azo dyes mineralization: Effect of  
454 current density,  $Fe^{2+}$  and dye concentration. *Chem. Eng. J.* 171, 385-392.

455 Salazar, R., Brillas, E., Sirés, I., 2012. Finding the best  $Fe^{2+}/Cu^{2+}$  combination for the solar  
456 photoelectro-Fenton treatment of simulated wastewater containing the industrial textile  
457 dye Disperse Blue 3. *Appl. Catal. B: Environ.* 115-116, 107-116.

458 Sirés, I., Brillas, E., Oturan, M.A., Rodrigo, M.A., Panizza, M., 2014. Electrochemical  
459 advanced oxidation processes: today and tomorrow. A review. *Environ. Sci. Pollut. Res.*  
460 21, 8336-8367.

461 Steter, J.R., Brillas, E., Sirés, I., 2016. On the selection of the anode material for the  
462 electrochemical removal of methylparaben from different aqueous media. *Electrochim.*  
463 *Acta* 222, 1464-1474.

464 Thiam, A. Brillas, E., Centellas, F., Cabot, P.L., Sirés, I., 2015a. Electrochemical reactivity of  
465 Ponceau 4R (food additive E124) in different electrolytes and batch cells. *Electrochim.*  
466 *Acta* 173, 523-533.

467 Thiam, A., Sirés, I., Brillas, E., 2015b. Treatment of a mixture of food color additives (E122,  
468 E124 and E129) in different water matrices by UVA and solar photoelectro-Fenton.  
469 *Water Res.* 81, 178-187.

470 Umar, M., Roddick, F., Fan, L., Aziz, H.A., 2013. Application of ozone for the removal of  
471 bisphenol A from water and wastewater - A review. *Chemosphere* 90, 2197-2207.

472 Xiang, G., Yu, Z., Hou, Y., Chen, Y., Peng, Z., Sun, L., Sun, L., 2016. Simulated solar-light  
473 induced photoelectrocatalytic degradation of bisphenol-A using Fe<sup>3+</sup>-doped TiO<sub>2</sub>  
474 nanotube arrays as a photoanode with simultaneous aeration. *Sep. Purif. Technol.* 161,  
475 144-151.

476 Yang, C., 2015. Degradation of bisphenol A using electrochemical assistant Fe(II)-activated  
477 peroxydisulfate process. *Water Sci. Eng.* 8, 139-144.

478 Yang, L., Li, Z., Jiang, H., Jiang, W., Su, R., Luo, S., Luo, Y., 2016. Photoelectrocatalytic  
479 oxidation of bisphenol A over mesh of TiO<sub>2</sub>/graphene/Cu<sub>2</sub>O. *Appl. Catal. B: Environ.*  
480 183, 75-85.

481

482 **Figure captions**

483 **Fig. 1.** Change of (a) TOC and (b) mineralization current efficiency with electrolysis time  
484 during the treatment of 150 mL of 0.556 mM bisphenol A in 0.050 M Na<sub>2</sub>SO<sub>4</sub> at pH 3.0 using  
485 a boron-doped diamond (BDD)/air-diffusion cell (3 cm<sup>2</sup> electrode area) at  $j = 33.3 \text{ mA cm}^{-2}$   
486 and 35 °C. Method: (●) Electrochemical oxidation with electrogenerated H<sub>2</sub>O<sub>2</sub> (EO-H<sub>2</sub>O<sub>2</sub>),  
487 (■) electro-Fenton (EF) with 0.50 mM Fe<sup>2+</sup> and (▲) photoelectro-Fenton (PEF) with 0.50  
488 mM Fe<sup>2+</sup> using a 6 W UVA lamp.

489 **Fig. 2.** Time course of (a,c) TOC and (b,d) mineralization current efficiency during the  
490 degradation of 150 mL of bisphenol A solutions in 0.050 M Na<sub>2</sub>SO<sub>4</sub> at pH 3.0 and 35 °C  
491 using a BDD/air-diffusion cell at  $j = 100 \text{ mA cm}^{-2}$ . (a,b) 0.556 mM bisphenol A treated by:  
492 (●) EO-H<sub>2</sub>O<sub>2</sub> and (■) EF, (▲) PEF and (▼) solar photoelectro-Fenton (SPEF) with 0.50  
493 mM Fe<sup>2+</sup>. (c,d) PEF process with: (●) 0.112 mM, (■) 0.278 mM, (▼) 0.417 mM and (▲)  
494 0.556 mM bisphenol A.

495 **Fig. 3.** Variation of (a) TOC and (b) mineralization current efficiency with electrolysis time  
496 for the treatment of 150 mL of 0.556 mM bisphenol A in 0.008 M NaCl + 0.047 M Na<sub>2</sub>SO<sub>4</sub> at  
497 pH 3.0 using a BDD/air-diffusion cell at  $j = 33.3 \text{ mA cm}^{-2}$  and 35 °C. Method: (●) EO-H<sub>2</sub>O<sub>2</sub>,  
498 (■) EF and (▲) PEF.

499 **Fig. 4.** (a,c) TOC and (b,d) mineralization current efficiency vs. electrolysis time under the  
500 same conditions of Fig. 2 but using 0.008 M NaCl + 0.047 M Na<sub>2</sub>SO<sub>4</sub> as electrolyte. (a,b)  
501 0.556 mM bisphenol A treated by: (●) EO-H<sub>2</sub>O<sub>2</sub>, (■) EF, (▲) PEF and (▼) SPEF. (c,d) PEF  
502 process with: (●) 0.112 mM, (■) 0.278 mM, (▼) 0.417 mM and (▲) 0.556 mM bisphenol  
503 A.

504 **Fig. 5.** Time course of bisphenol A concentration during the degradation of 150 mL of 0.556  
505 mM bisphenol A in different electrolytes at pH 3.0 using a BDD/air-diffusion cell at  $j = 100$   
506 mA cm<sup>-2</sup> and 35 °C. (a) EO-H<sub>2</sub>O<sub>2</sub> with 0.008 M NaCl + 0.047 M Na<sub>2</sub>SO<sub>4</sub>. (b) SPEF with (▼)  
507 0.050 M Na<sub>2</sub>SO<sub>4</sub> and (○) 0.008 M NaCl + 0.047 M Na<sub>2</sub>SO<sub>4</sub>. The inset panels present the  
508 corresponding pseudo-first-order kinetic analysis.

509 **Fig. 6.** Initial reaction sequence proposed for bisphenol A degradation in the Cl-containing  
510 matrix by EAOPs.  $\bullet\text{OH}$  accounts for hydroxyl radicals originated at the anode surface and  
511 from Fenton's reaction, whereas  $\text{HClO}$  accounts for active chlorine formed from  $\text{Cl}^-$  oxidation  
512 at the anode.

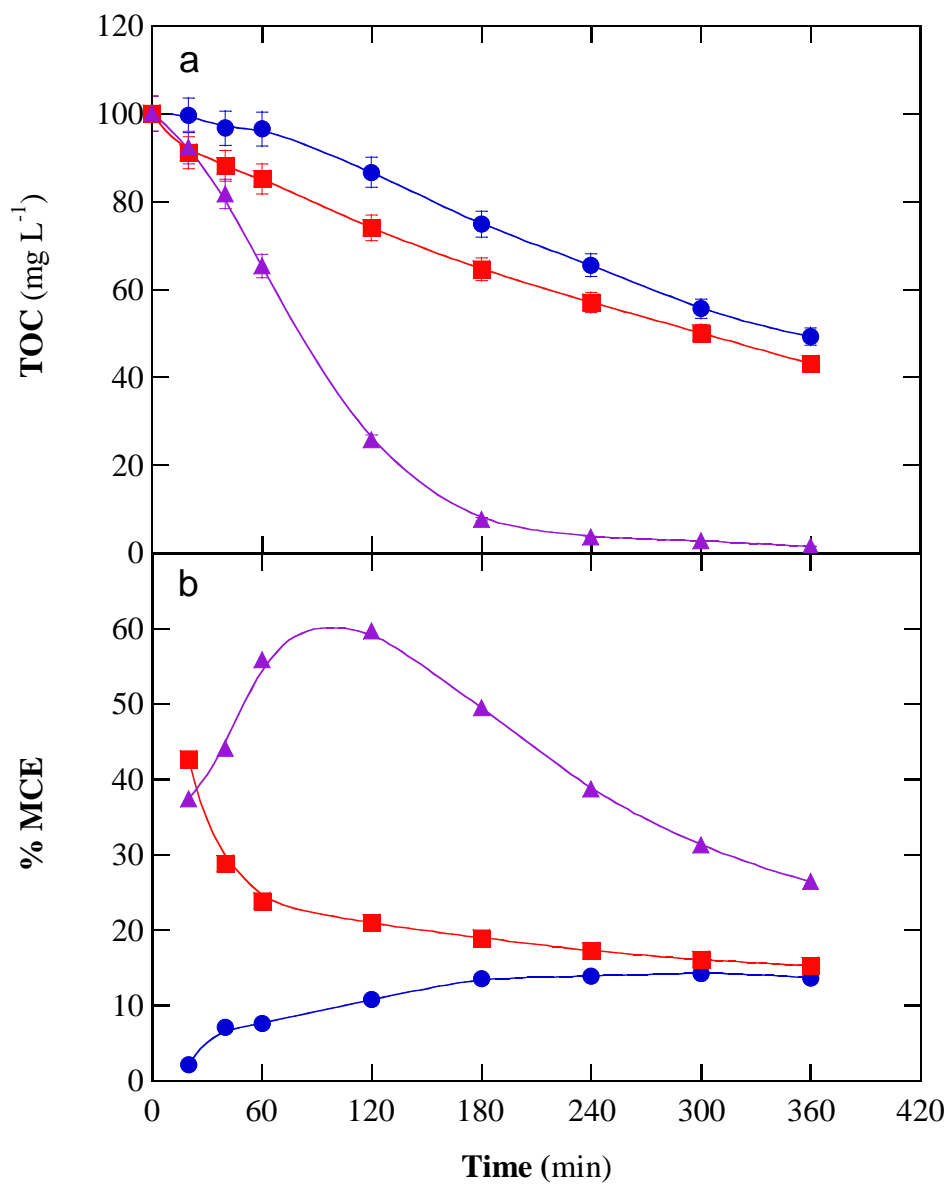


**Fig. 1**



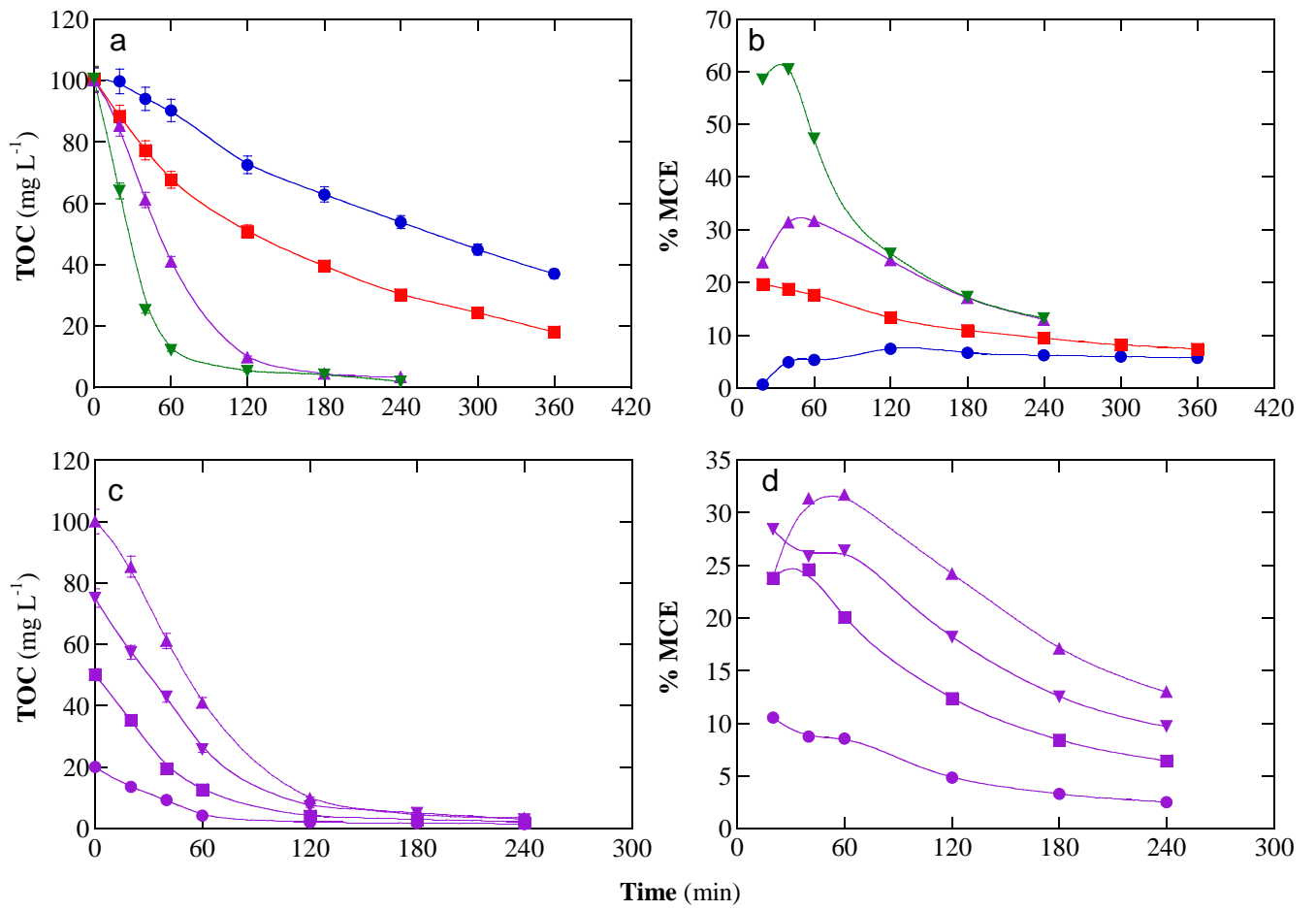


**Fig. 2**

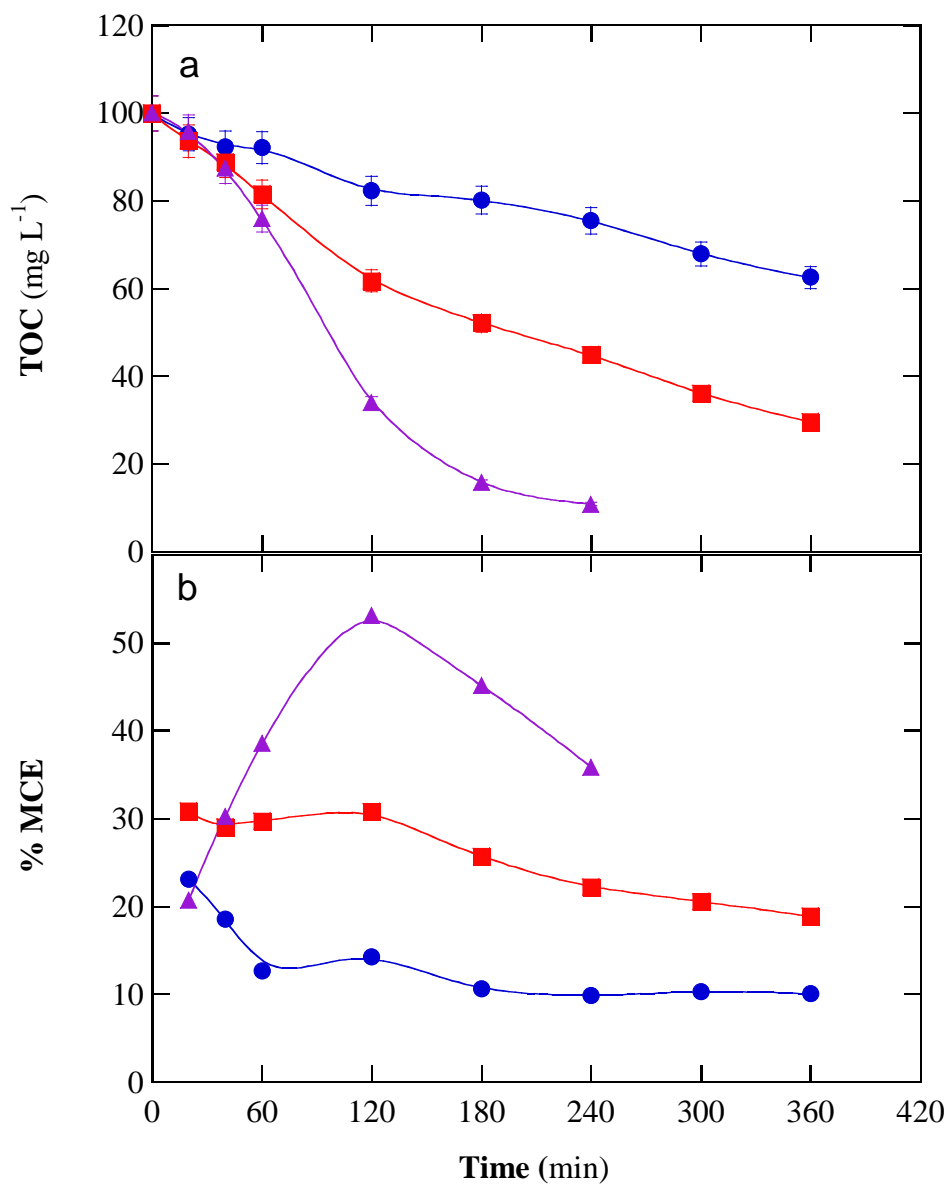


**Fig. 3**

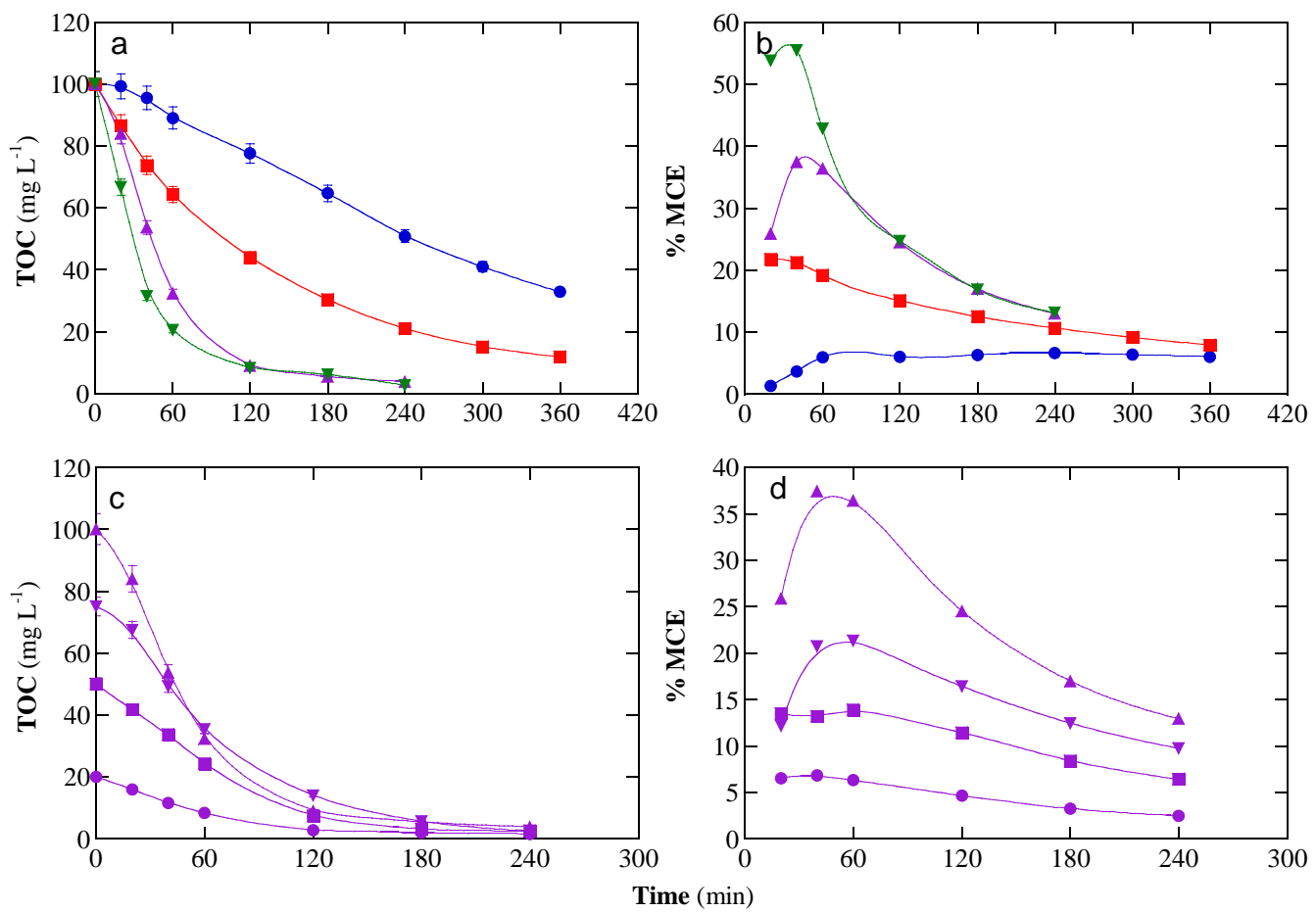


**Fig. 4**

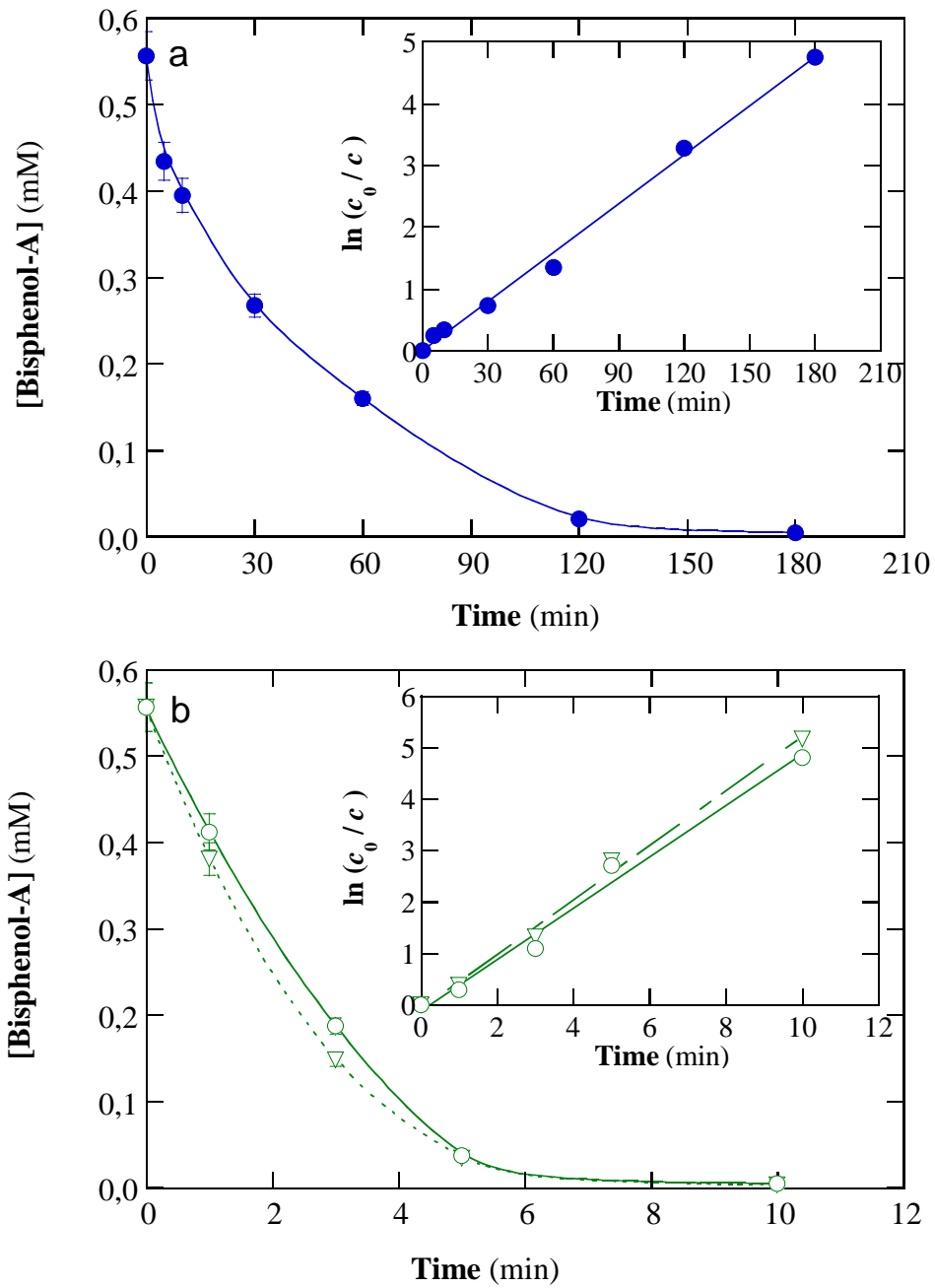


**Fig. 5**

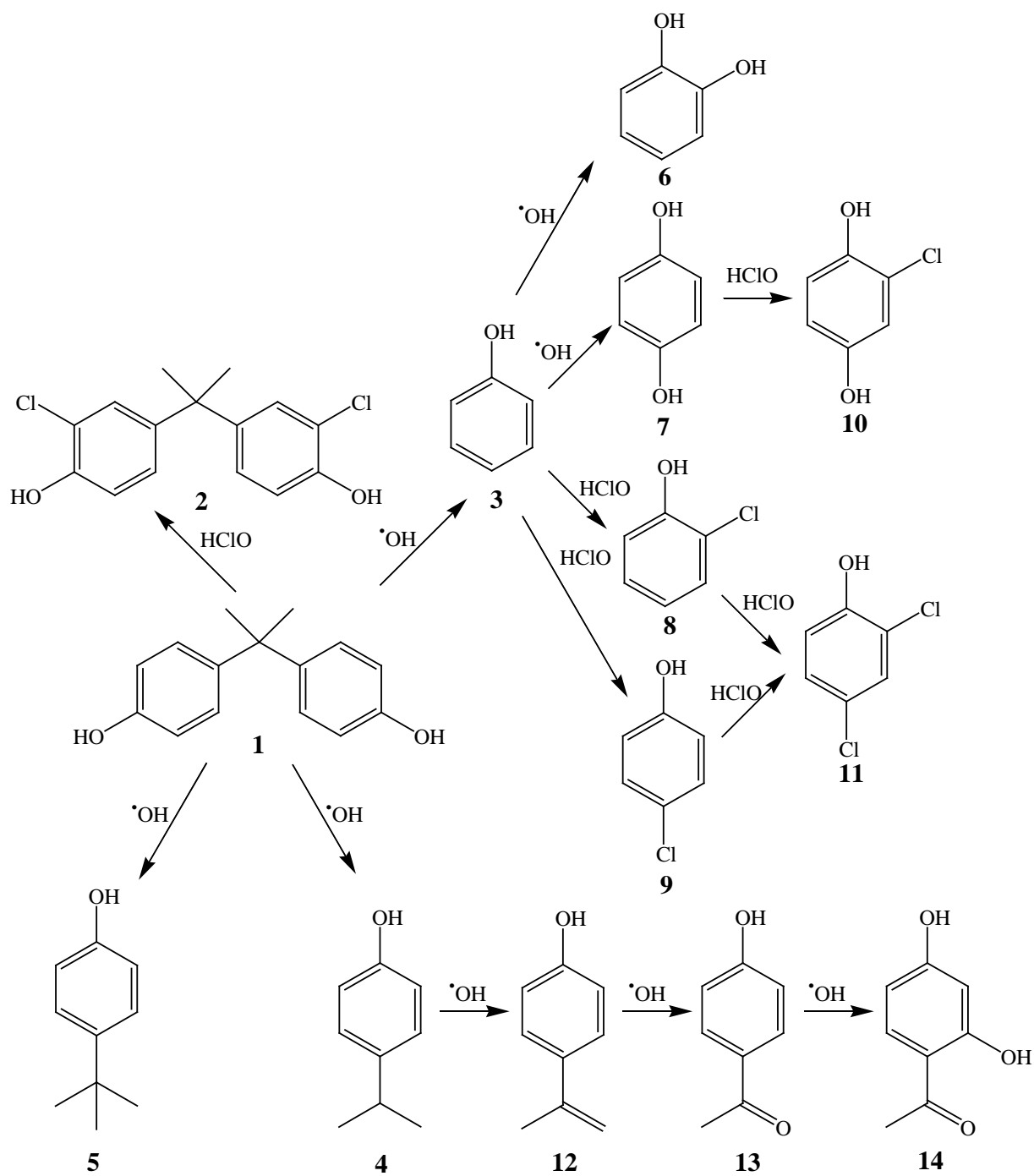


Fig. 6

**Table 1.**

Pseudo-first-order rate constant obtained for TOC removal ( $k_{\text{TOC}}$ ) and the corresponding  $R$ -squared, and percentage of TOC removal and mineralization current efficiency at 240 min. Trials were made using 150 mL of bisphenol A solutions in different matrices at pH 3.0 and 35 °C with different electrolytes by several EAOPs with a BDD/air-diffusion cell.

Method	[Bisphenol A] <sub>0</sub> (mM)	$j$ (mA cm <sup>-2</sup> )	$k_{\text{TOC}}$ (min <sup>-1</sup> )	$R^2$	% TOC removal	% MCE
<i>0.050 M Na<sub>2</sub>SO<sub>4</sub></i>						
EO-H <sub>2</sub> O <sub>2</sub>	0.556	33.3	2.0×10 <sup>-3</sup>	0.985	34.6	13.9
	0.556	100	2.8×10 <sup>-3</sup>	0.996	46.2	6.2
EF <sup>a</sup>	0.556	33.3	2.3×10 <sup>-3</sup>	0.998	43.0	17.3
	0.556	100	4.6×10 <sup>-3</sup>	0.995	69.8	9.4
PEF <sup>a,b</sup>	0.556	33.3	1.3×10 <sup>-2</sup>	0.980	96.3	38.7
	0.112	100	2.3×10 <sup>-2</sup>	0.979	93.2	2.5
	0.278	100	2.1×10 <sup>-2</sup>	0.994	95.9	6.4
	0.417	100	2.0×10 <sup>-2</sup>	0.995	96.3	9.7
	0.556	100	1.9×10 <sup>-2</sup>	0.987	96.6	12.9
SPEF <sup>a,c</sup>	0.556	100	3.6×10 <sup>-2</sup>	0.985	98.2	13.2
<i>0.008 M NaCl + 0.047M Na<sub>2</sub>SO<sub>4</sub></i>						
EO-H <sub>2</sub> O <sub>2</sub>	0.556	33.3	1.2×10 <sup>-3</sup>	0.986	23.5	9.8
	0.556	100	3.1×10 <sup>-3</sup>	0.990	49.2	6.6
EF <sup>a</sup>	0.556	33.3	3.4×10 <sup>-3</sup>	0.996	55.2	22.2
	0.556	100	6.0×10 <sup>-3</sup>	0.985	79.1	10.6
PEF <sup>a,b</sup>	0.556	33.3	1.0×10 <sup>-2</sup>	0.981	89.1	35.8
	0.112	100	1.7×10 <sup>-2</sup>	0.994	92.0	2.4
	0.278	100	1.6×10 <sup>-2</sup>	0.983	95.2	6.5
	0.417	100	1.5×10 <sup>-2</sup>	0.997	96.0	9.6
	0.556	100	1.4×10 <sup>-2</sup>	0.990	96.1	12.8
SPEF <sup>a,c</sup>	0.556	100	2.8×10 <sup>-2</sup>	0.985	97.4	13.1

<sup>a</sup> Addition of 0.50 mM Fe<sup>2+</sup>

<sup>b</sup> Upon 6 W UVA irradiation

<sup>c</sup> Upon sunlight irradiation